11-5-2020

Substrate–Support Interactions Mediate Hydrogenation of Phenolic Compounds by Pd/CeO2 Nanorods

Yeongseo An
Iowa State University, yan1@iastate.edu

Pranjali Naik
Iowa State University and Ames Laboratory, naikpj@iastate.edu

Igor I. Slowing
Iowa State University and Ames Laboratory, islowing@iastate.edu

Vincenzo Venditti
Iowa State University, venditti@iastate.edu

Substrate–Support Interactions Mediate Hydrogenation of Phenolic Compounds by Pd/CeO2 Nanorods

Abstract

Ceria-supported palladium (Pd/CeO2) has spawned significant attention in recent years due to its ability to catalyze selective hydrogenation of phenolic compounds to cyclohexanones and cyclohexanols at a mild temperature and pressure. However, the mechanistic basis by which ceria enhances catalytic conversion is still unclear. Here, we use the increase in the 13C transverse relaxation rate upon the addition of nanoparticles (NPs) (13C $\Delta R2$) to investigate the adsorption of phenolic compounds on the surface of the Pd/CeO2 catalyst by solution NMR. We show that hydroxyphenols adsorb on the support more efficiently than underivatized phenol and methoxyphenols and that phenol derivatives with an oxygen atom at position 2 (i.e., 2-hydroxyphenol and 2-methoxyphenol) form very stable interactions with the Pd site of Pd/CeO2. An analysis of the kinetics of hydrogenation revealed that catalytic conversion is linearly correlated with the ability of the substrate to form interactions with the CeO2 support and is inhibited by the formation of stable substrate–Pd adducts. Our data suggest that CeO2–substrate interactions mediate phenol hydrogenation more efficiently than Pd–substrate interactions and explain the exceptional catalytic performance reported for Pd/CeO2.

Keywords

surface contrast NMR, sorption equilibria, heterogeneous catalysis, NMR relaxation, hydrogen bonding

Disciplines

Materials Chemistry | Nanoscience and Nanotechnology

Comments

Substrate-Support Interactions Mediate Hydrogenation of Phenolic Compounds by Pd/CeO_2 Nanorods

Yeongseo An,[1,†] Pranjali Naik,[1,2,†] Igor I. Slowing,[1,2,] and Vincenzo Venditti[1,3,*]

[1] *Department of Chemistry, Iowa State University, Ames, Iowa 50011, USA.*

[2] *U.S. Department of Energy, Ames Laboratory, Ames, IA 50011, USA.*

[3] *Roy J. Carver Department of Biochemistry, Biophysics and Molecular Biology, Iowa State University, Ames, Iowa 50011, USA.*

[*] Address correspondence to:

Vincenzo Venditti, Department of Chemistry, Iowa State University, Hach Hall, 2438 Pammel Drive, Ames, IA 50011, USA. email: venditti@iastate.edu; Tel. 515-294-1044; Fax: 515-294-7550; ORCID 0000-0001-8734-0400.

[†] Y. A. and P. N. contributed equally to this work.

Abstract

Ceria-supported palladium (Pd/CeO_2) has spawned significant attention in recent years due to its ability to catalyze selective hydrogenation of phenolic compounds to cyclohexanones and cyclohexanoles at mild temperature and pressure. However, the mechanistic basis by which ceria enhances catalytic conversion is still unclear. Here, we use the increase in ^{13}C transverse relaxation rate upon the addition of nanoparticle (NP) ($^{13}C\ \Delta R_2$) to investigate the adsorption of phenolic compounds to the surface of the Pd/CeO_2 catalyst by solution NMR. We show that hydroxyphenols adsorb on the support more efficiently than underivatized phenol and methoxyphenols, and that phenol derivatives with an oxygen atom at position 2 (i.e. 2-hydroxyphenol and 2-methoxyphenol) form very stable interactions with the Pd site of Pd/CeO_2. Analysis of the kinetics of hydrogenation revealed that catalytic conversion is linearly correlated to the ability of the substrate to form interactions with the CeO_2 support and is inhibited by the formation of stable substrate-Pd adducts. Our data suggest that CeO_2-substrate interactions mediate phenol hydrogenation more efficiently than Pd-substrate interactions, and explain the exceptional catalytic performance reported for Pd/CeO_2.

Keywords

Surface Contrast NMR; sorption equilibria; heterogeneous catalysis; NMR relaxation; hydrogen bonding

Introduction

Nanoparticles (NPs) have found application in various fields such as chemical, energy, and petrochemical industries as heterogeneous catalysts.[1-2] Since NP catalysis is a surface-based process, understanding the interactions between the substrate and the surface is of paramount importance. We have recently shown that surface contrast (SC) solution NMR methods, such as dark-state exchange saturation transfer (DEST)[3-4] and relaxation dispersion (RD)[5-6] experiments, can be used to characterize the structures, kinetics, and thermodynamics of sorption equilibria with atomic resolution.[7-8] In particular, by using the interaction between aqueous phenol (PhOH) and ceria-supported palladium NPs (Pd/CeO_2) as a model system, we showed that PhOH adsorption on the metal proceeds via a weakly bound intermediate state in which the small molecule is hydrogen-bonded to the ceria support.[7] It is important to notice that the DEST experiment used in our previous investigation[7] differs from the Saturation Transfer Difference (STD)-NMR method used by Zhang et al.[9] to investigate surface adsorption. Indeed, DEST does not rely on the transfer of magnetization from the NP to the small molecule adsorbate. Therefore, DEST is better suited than STD to investigate adsorption on metal and metal-oxide NPs.

Pd/CeO_2 catalyzes selective hydrogenation of PhOH to cyclohexanone and cyclohexanol under mild reaction conditions (1 bar H_2 at 35 °C).[10] In this hierarchical catalytic system, palladium is crucial for hydrogen adsorption and activation, while ceria facilitates PhOH adsorption and Pd dispersion.[10] However, it is not clear if catalysis occurs at the Pd site or there is a direct participation of ceria in catalysis via H_2 spillover. Interestingly, by comparing SC NMR and reaction kinetic data measured in the presence and in the absence of a phosphate buffer (that forms strong interactions with ceria), we showed that destabilization of the PhOH-ceria interaction proportionally decreases the rate of catalytic conversion.[7] As the observed rate of a catalyzed reaction is directly proportional to the concentration of reactant-catalyst complex,[11] our data provided strong experimental evidence that weak interactions between PhOH and ceria are catalytically competent, and offer a clear example of how SC NMR data can guide the interpretation of reaction kinetic experiments.

One possible curb of SC NMR methods is that they usually require extensive NMR data acquisition and the use of not-trivial analysis protocols that might limit their widespread use in interfacial science. Indeed, simultaneous fitting of multiple SC NMR experiments using Bloch-McConnell theory is often required in order to accurately determine kinetic,

thermodynamic, and structural parameters of sorption equilibria involving exchange among several adsorbed species (such as, for example, the equilibrium between weakly and tightly adsorbed state of PhOH on Pd/CeO_2). Herein, we show that ^{13}C ΔR_2 values, which are obtained by taking the difference between the ^{13}C transverse relaxation rate (R_2) measured for the small molecule in the presence and absence of NP, can be used to investigate small molecule adsorption in a simple and semiquantitative manner. We test this approach by investigating the adsorption of PhOH and of its hydroxy and methoxy derivatives on the surface of CeO_2 and Pd/CeO_2 nanorods (Figure 1 and Supporting Figure S1). We show that the hydroxyphenols interact with the ceria support more efficiently than PhOH and methoxyphenols. In addition, we observe that introduction of the oxygen at position 2 stabilizes the interaction between Pd and the small molecule and results in a significant drop in catalytic conversion. Our data confirm our previous observation that interactions between PhOH and support are competent for the hydrogenation reaction.[7] Furthermore, we demonstrate that strong Pd-substrate interactions inhibit catalytic conversion, and we provide one additional example of the use of SC NMR in addressing fundamental questions in heterogeneous catalysis.

Results and discussion

Synthesis of Pd/CeO_2 nanorods. CeO_2 nanorods were prepared in highly basic media (10 M NaOH) under hydrothermal conditions (100 °C)(Figure 1a).[12] The combination of high OH^- concentration and high temperature under autogenic pressure induces anisotropic growth of the primary $Ce(OH)_3$ nuclei along the [110] direction and ripening via dissolution/recrystallization.[13-14] Oxidation by dissolved O_2 and exposure to air resulted in CeO_2 nanorods that presented predominantly (110) and (100) facets in agreement with the literature (Figure 1b,c).[12, 15] Pd nanoparticles were produced on the nanorods via incipient wetness impregnation of $Pd(OAc)_2$ followed by calcination and reduction under H_2 flow at 350 °C (Figure 1d). TEM imaging of the materials indicated that formation of Pd nanoparticles induced partial sintering and some extent of restructuring of the CeO_2 rods, as the average diameters increased from ca. 10 nm in the original material to about 20-40 nm, and the edges of the particles became more rounded (Figure 1e). These changes in particle morphology have been observed before,[16-17] and are consistent with a decrease in the specific surface area from 69 m^2/g to 39 m^2/g, as well as a growth in the CeO_2 crystallite size from ca. 10 nm to 25 nm as estimated from their XRD patterns using the Scherrer equation (Supporting Figure S2 and Supporting Table S1). In spite of these changes, HR TEM revealed the surface of the Pd/CeO_2 remained predominantly

terminated in defect rich (110) and (100) planes (Figure 1f). Because of its lower Z contrast relative to Ce it was difficult to observe Pd nanoparticles under the TEM. Pd nanoparticle size was estimated from a few regions where they were visible giving values around 1.4 nm (Supporting Figure S3). This result is consistent with the average Pd crystallite size obtained from sub-ambient pulsed H_2 chemisorption (1.3 nm).

Guide to interpretation of ^{13}C ΔR_2 data. In the present work experimental ^{13}C ΔR_2 parameters are used to investigate the adsorption of phenolic compounds on the surface of CeO_2 and Pd/CeO_2 nanorods. The value of ΔR_2 is a convoluted function of the R_2's and thermodynamic populations of the desorbed and adsorbed states, and of the rates of exchange among these states.[18] As such, quantitative modelling of the experimental ΔR_2 values requires solution of the Bloch-McConnell equation. However, if predictive structural models of the adsorbed states are available, information on the surface-bound states can be inferred from the ^{13}C ΔR_2 values without the need of complicated mathematical modelling. The main theoretical assumptions are that ^{1}H-^{13}C dipolar coupling and Chemical Shift Anisotropy (CSA) are the principal relaxation mechanisms determining the ^{13}C R_2 of free and NP-bound states of the small molecule, and that rotational diffusion of the C-H bond vectors is the main source of modulation of the local magnetic fields (inducing relaxation of the NMR signals) at the ^{13}C atom. Under these conditions, the observed ^{13}C R_2's are inversely proportional to the rotational diffusion of the individual C-H bond vectors.[7, 18]

In the case of PhOH adsorption on Pd/CeO_2, three major binding modes have been reported: (i) hydrogen-bonding to ceria via the hydroxyl group (Figure 2a),[7, 10] (ii) flat adsorption on the Pd NP (Figure 2b),[7, 19] and (iii) binding to an oxygen vacancy on the ceria support (Figure 2c).[7, 10] In binding mode (i), the three rotatable bonds separating the aromatic group from the surface of ceria confer great conformational freedom to PhOH. In such case, all C-H bonds reorient relative to the external magnetic field with similar rotational correlation time (τ_{loc}) and experience similar increase in ^{13}C R_2 upon binding. In binding mode (ii), PhOH is rigidly attached to the NP surface. This condition results in all C-H bonds to reorient with the same rotational correlation time as the NP (τ_{NP}) and experience similar ^{13}C ΔR_2 upon binding (note that similar conclusions can be drawn for PhOH bound at the interface between Pd and CeO_2, which would be indistinguishable from binding mode (iii) in our experiments). Finally, the presence of a single rotatable bond in binding mode (iii) generates a dependency of the ^{13}C R_2 from the angle θ formed by the

C-H bond vector and the axis of rotation that can be modelled by a $Y_2^0(\theta,\varphi)$ spherical harmonic (Figure 2d).[7, 20-21] Indeed, a C-H bond aligned with the axis of rotation (the para C-H bond in the case of PhOH bound to an oxygen vacancy on CeO_2, Figure 2c,d) will appear as rigidly attached to the NP (i.e. it will tumble with rotational correlation time ~ τ_{NP}) and will result in a maximum ^{13}C R_2. Conversely, deviation of the C-H bond from the axis of rotation will introduce additional modulation of the local magnetic fields that will reduce the ^{13}C transverse relaxation and will result in ^{13}C R_2 minima (corresponding to the R_2 measured for the free state) when θ corresponds to the magic angles (54.74° and 125.26°).[7, 20-21] Therefore, for an NMR sample of PhOH and Pd/CeO_2 in which binding modes (i)-(iii) coexist, the observed ^{13}C ΔR_2 can be modelled using the formula $\Delta R_2(\theta) = R_{iso} + R_{ani}[Y_2^0(\theta,\varphi)]^2$, where R_{iso} is a scaling factor that depends on the amount of PhOH in binding modes (i) and (ii) and R_{ani} is a scaling factor that depends on the amount of PhOH in binding mode (iii) (Figure 2e).

Finally, it is important to notice that the relationship between the parameters R_{iso} and R_{ani} and the fractional populations of PhOH in binding modes (i)-(iii) depends on the rotational diffusion of the small molecule. As the PhOH complexes in Figures 2a-c display different degrees of local flexibility, direct comparisons between R_{iso} and R_{ani} or between R_{iso} parameters measured in the presence of CeO_2 (where mode (i) is the only contribution to R_{iso}) and in the presence of Pd/CeO_2 (where both binding modes (i) and (ii) contribute to R_{iso}) are not possible. On the other hand, comparisons among R_{iso} and R_{ani} measured for similar small molecules upon the addition of identical NPs is a rapid and convenient way to investigate their relative affinity for the NP surface.

Adsorption of phenolic compounds on CeO_2 nanorods. ^{13}C ΔR_2 measured for PhOH, anisole, and the hydroxy and methoxy derivatives of PhOH upon the addition of CeO_2 nanorods are reported as a function of θ in Figure 3. As the NMR sequence used to measure the ^{13}C R_2 data employs two refocused-INEPT blocks to increase the sensitivity of the experiment,[7] relaxation data were only measured for C atoms covalently attached to one hydrogen. Data measured for PhOH, 2-hydroxy, 3-hydroxy, and 3-methoxy phenols were modelled by optimizing the values of R_{iso} and R_{ani}. When a reliable measure of the ^{13}C ΔR_2 value for θ = 0° could not be obtained because of signal overlap (i.e. in case of anisole and 2-methoxyphenol – Supporting Figure S4) or because of the absence of a CH group in para respect to the OH group (i.e. in case of 4-hydroxyphenol and 4-

methoxyphenol), only the R_{iso} parameter was used for data modelling. Optimized values of R_{iso} and R_{ani} are listed in Table 1.

The ΔR_2 data measured for PhOH in the presence of the CeO_2 nanorods show the same overall trend observed previously for PhOH adsorption on CeO_2 nanocubes,[7] with the para position displaying larger ΔR_2 than the ortho and meta positions (Figure 3). This pattern indicates that binding modes (i) and (iii) coexist on the surface of the NP. Of notice, similar data measured for anisole (methoxybenzene) indicate that addition of CeO_2 has little to no effect on the transverse relaxation rate (Figure 3), which reveals that anisole is incapable to hydrogen bond to the NP and that PhOH acts as the H-bond donor in its complex with CeO_2.

The addition of a second OH group to PhOH results in an overall increase in ΔR_2 (Figure 3). Interestingly, modelling the experimental data measured for the hydroxy derivatives of PhOH upon addition of CeO_2 returns R_{iso} parameters that are ~2 times larger and R_{ani} parameters that are ~2 times smaller than the ones obtained for non-derivatized PhOH in the presence of CeO_2 (Figures 4a,c). This increase in R_{iso} reflects the fact that hydroxy phenols are two times more likely than PhOH to hydrogen-bond to ceria via random collisions, which increases the effective population of binding mode (i) in the sample. In contrast, the reduction in R_{ani} cannot be ascribed to a destabilization of binding mode (iii), but it is rather due to an ambiguous definition of para C in hydroxyphenols. Indeed, if we take the case of the 2-hydroxyphenol as an example, the H4-C4 bond is positioned on the axis of internal rotation (θ = 0°) and the C4 nucleus experiences enhanced R_2 relaxation when O1 interacts with an oxygen vacancy on ceria. However, if the interaction with the vacant site occurs via the O2, the H4-C4 bond forms an angle of 60° with the axis of internal rotation, and the C4 nucleus experiences an R_2 similar to one measured for the desorbed molecule. As a result of this ambiguity in the definition of the para position, the R_{ani} measured for the hydroxyphenols is expected to be roughly one-half of the one measured for non-derivatized PhOH or for phenolic compounds that cannot form multiple interactions with oxygen vacant sites. ΔR_2 data acquired on methoxyphenols upon the addition of CeO_2 confirm the interpretation given above for the R_{iso} and R_{ani} parameters of the hydroxyphenols. Indeed, the substitution of one OH moiety with an OCH_3 group, which cannot interact with surface exposed oxygen vacancies nor hydrogen bond to ceria (note that anisole does not interact with CeO_2, Figures 3 and 4), returns R_{iso} and R_{ani} parameters identical within error to the ones measured for underivatized PhOH.

Adsorption of phenolic compounds on Pd/CeO$_2$. ^{13}C ΔR_2 measured for PhOH, anisole, and the hydroxy and methoxy derivatives of PhOH upon the addition of Pd/CeO$_2$ are shown in Figure 3. As discussed above (see "*Guide to interpretation of ^{13}C ΔR_2 data"*) a direct comparison of the ΔR_2's measured upon addition of CeO$_2$ and Pd/CeO$_2$ is not possible due to the fact that the two NPs interact differently with phenolic compounds, and that the small molecules experience different local dynamics when adsorbed on their surface.

Interestingly, the ΔR_2 data measured for PhOH and its derivatives in the presence of Pd/CeO$_2$ show a dependency on the θ angle that is characteristic of an interaction with an oxygen vacant site (i.e. ΔR_2 for the para position is larger than for the ortho and meta position) (Figure 3). This observation contrasts with the ΔR_2 data we have recently published for PhOH adsorption on Pd/CeO$_2$ of cubic morphology.[7] Indeed, in our previous publication, we reported no dependency of ΔR_2 on the angle θ. We interpreted the measurement of homogeneous ΔR_2 across the small molecule as an indication that the formation of the Pd sites on the surface of the ceria nanocubes resulted in a near-complete elimination of all oxygen vacancies from the support.[7] As CeO$_2$ nanorods are known to contain more defects than CeO$_2$ of cubic morphology,[22-23] we ascribe the ΔR_2 dependency on θ observed here to the persistence of a significant number of oxygen vacancies on the Pd/CeO$_2$ nanorods. However, it should be noted that, as the morphology affects both surface termination of the NP (i.e. (110) and (100) for rod and cubic morphology, respectively) and acidic strength of Ce atoms,[24-25] additional structural factors might contribute to the persistence of anisotropy in the ΔR_2 data measured in the presence of Pd/CeO$_2$ nanorods.

Optimized R_{iso} and R_{ani} from the modelling of the ΔR_2 data are reported in Figure 4 and Table 1. Consistent with the data measured in the presence of CeO$_2$ nanorods, the R_{ani} parameters obtained for 2- and 3-hydroxyphenol are about two times smaller than the ones obtained for PhOH and 3-methoxyphenol (Figure 4c), confirming that binding mode (iii) is the major cause of anisotropy in the ^{13}C ΔR_2 data. On the other hand, in the presence of Pd/CeO$_2$, the derivatization of PhOH with a second OH group does not result in a homogeneous doubling of R_{iso} as observed in the presence of CeO$_2$ nanorods (Figure 4a). In particular, the R_{iso} measured for 2- and 4-hydroxyphenol is ~4 times larger than the one measured for PhOH, which indicates that these derivatized molecules adsorb on the NP surface more efficiently than 3-hydroxyphenol and PhOH. To investigate if the high affinity of 2- and 4-hydroxyphenol for Pd/CeO$_2$ is the result of efficient adsorption on the Pd site

or is due to a stabilization of the hydrogen-bonding interaction with CeO_2 due to the presence of Pd (note that both binding modes (i) and (ii) contribute to R_{iso}), additional ΔR_2 experiments were acquired on 2-, 3-, and 4-methoxyphenol in the presence of Pd/CeO_2. As the OCH_3 group is incapable of interacting efficiently with CeO_2, we expect the methoxyphenols to have the same ability as PhOH to hydrogen-bond to Pd/CeO_2 via binding mode (i). Of note, while 4-methoxyphenol has low R_{iso} similar to PhOH, 2-methoxyphenol retains the high R_{iso} observed for its hydroxy analogue (Figure 4a), suggesting that the oxygen at position 2 increases the ability of phenolic compounds to adsorb to the Pd site of Pd/CeO_2.

Adsorption on Pd reduces the rate of hydrogenation. The analysis of the NMR data presented above indicated that Pd/CeO_2 adsorbs PhOH and its hydroxy and methoxy derivatives with stunningly different affinities. To investigate the relationship between surface adsorption and catalytic conversion, the rate of hydrogenation of PhOH, anisole, and the hydroxy and methoxy derivatives of PhOH catalyzed by 1 wt% Pd/CeO_2 nanorods was measured at 35 °C and 1 bar H_2 as described in *Experimental methods*. % conversions obtained after 7 h of incubation with the NP catalyst are plotted versus the experimental R_{iso} and R_{ani} parameters measured for the small molecules upon addition of Pd/CeO_2 in Figures 4b,d. In these plots, the R_{ani} values measured for 2- and 3-hydroxyphenol are multiplied by 2 in order to account for the ambiguity in the definition of the para carbon of hydroxyphenols (see above).

Analysis of Figures 4b and d reveals that the % conversion is linearly correlated with the R_{iso} and R_{ani} parameters derived by NMR, indicating that the rate of hydrogenation depends on the amount of substrate adsorbed on the surface of the catalyst. It is interesting to note that significant exceptions to the linear correlation trend are only observed for 2-hydroxyphenol and 2-methoxyphenol. Indeed, despite a very high affinity for the NP surface (revealed by the large values of R_{iso} and R_{ani}), these two molecules are hydrogenated very inefficiently by the catalyst, consistently with what previously reported by us.[26] Since our NMR analysis indicated that 2-hydroxyphenol and 2-methoxyphenol possess much higher affinity for Pd sites than the other phenolic compounds investigated here, our data suggest that formation of a stable substrate-Pd interaction inhibits catalytic hydrogenation of phenolic compounds by Pd/CeO_2.

Conclusion

Here, we have used ^{13}C ΔR_2 data to investigate the adsorption of phenolic compounds on the surface of Pd/CeO_2 nanorods. We have shown that the ability of the small molecules to adsorb to ceria depends on the number of OH groups, with hydroxyphenols adsorbing to the surface more efficiently than PhOH and methoxyphenols. In addition, our data revealed that methoxy groups are not capable of effectively hydrogen-bonding to ceria and that PhOH derivatives with an O atom at position 2 form very stable adducts with the Pd sites of Pd/CeO_2.

A comparison of the NMR data with the rate of catalytic hydrogenation measured for the phenolic compounds in the presence of Pd/CeO_2 revealed that % conversion is linearly correlated with the amount of adsorbed small molecule but is inhibited by strong interactions between the substrate and the Pd sites. These data agree with our recent study indicating that the weak interactions between substrate and ceria are competent for catalysis,[7] and suggest that stable substrate-Pd adducts may compete with H_2 adsorption and activation and/or reduce catalytic conversion by reducing the rate of product release from the catalyst.

Finally, we have shown that ^{13}C ΔR_2 data provide important insight into sorption equilibria. Although they do not return the comprehensive kinetic, thermodynamic, and structural description of NP surface adsorption obtained by a rigorous analysis of a complete set of SC NMR experiments,[7] ^{13}C ΔR_2 measurements are less time-consuming and easier to analyze as they do not require extensive modelling and data fitting procedures. Therefore, ΔR_2 experiments are ideally suited to screen the affinity of libraries of small molecules against multiple NP targets.

Experimental methods

Synthesis of CeO_2 and Pd/CeO_2 nanorods. CeO_2 nanorods were synthesized using method from the literature.[12] In a Teflon bottle, 6.96 g of $Ce(NO_3)_3 \cdot 6H_2O$ was dissolved in 40 mL of deionized water. In a separate beaker, NaOH (115.2 g) was dissolved in 280 mL of deionized water. Then, NaOH (10 M) solution was added to the Teflon bottle, and the mixture was stirred for 30 min with the formation of a milky slurry. The Teflon bottle was placed in a stainless-steel vessel autoclave, set into a preheated oven (100 °C), and kept at 100 °C for 24 h. After the autoclave cooled down to room temperature, the solution was removed by centrifugation, washed with deionized water and ethanol 3 times, followed by drying in lypholizer overnight. The powder was then calcined at 450 °C for 4 h at 1 °C/min.

The Pd/CeO_2 catalyst was prepared by impregnation with a 1 wt % Pd loading relative to the mass of the support. The required amount of palladium acetate ($Pd(OAc)_2$) was dissolved in 5 mL of acetone. The solution was added dropwise into the CeO_2 support. Using mortar and pestle the catalyst was mixed thoroughly. The material was then calcined in air at 350 °C for 2 h, followed by reduction under H_2 flow (10 cm^3/min**)** at 350 °C for 2 h.

Transmission Electron Microscopy. NP imaging was performed in a FEI Tecnai G2 F20 field emission TEM operating at 200 kV. Samples were prepared by placing 3-4 drops of ethanol suspension (~0.1 mg mL-1) onto lacey-carbon-coated copper grids and dried in air.

Preparation of NMR Samples. NP suspensions were prepared in an agarose gel matrix, as previously described.[8] Briefly, substrate (10 mM), nanoparticles (1 wt%), and agarose (1 wt%) were mixed together and the pH of the solution was adjusted to ~7.0 using dilute HCl or NaOH. The mixture was then sonicated for 1 minute (1:2 on:off duty cycle) at 25% power on a 500W horn-tipped sonicator, heated to 75 °C for 10 minutes, transferred to a 5 mm NMR tube, and allowed to cool at room temperature for 10 to 15 minutes. Reference samples that did not contain nanoparticles were prepared using the same procedures as above. Phenol and agarose were purchased from Sigma-Aldrich. Anisole, hydroxyphenols, and methoxyphenols were purchased from Fisher Scientific. All chemicals were used without further purification.

NMR Spectroscopy. ^{13}C R_2 NMR data was collected at 25 °C on a Bruker 800 MHz spectrometer equipped with triple resonance z-gradient cryoprobe. ^{13}C R_2 was measured using a double INEPT-based CPMG sequence with proton decoupling during the ^{13}C relaxation period.[7] The ^{13}C carrier frequency was set at the center of the aromatic region of each molecule. The CPMG field strength was set to 1 kHz. For each sample, spectra at 14 different relaxation delays were acquired in an interleaved manner to obtain the ^{13}C R_2 relaxation decay curve. The observed relaxation decays were fitted to a monoexponential decay function $ae^{-R_2 t}$, where ***a*** is a scaling factor, R_2 is the transverse relaxation rate, and ***t*** is the variable relaxation delay. Experiments were acquired with 32 dummy scans and 128 scans with a recycle delay of 4 seconds between each scan. NMR spectra were processed and analyzed using Mnova NMR software

(http://mestrelab.com/software/mnova/nmr/). Experimental error was evaluated to be ≤ 5 % of the measured value by repeating the measurements.

Calculation and modelling of ^{13}C ΔR_2 data. Resonance specific ^{13}C ΔR_2 values were obtained by subtracting the ^{13}C R_2 measured for the small molecule in the absence of nanoparticles from the ^{13}C R_2 measured in the presence of 1 wt % nanoparticle. Errors on the ^{13}C ΔR_2 data were calculated propagating the errors on the ^{13}C R_2 values obtained experimentally (see "*NMR Spectroscopy*").

The ^{13}C ΔR_2 data were modelled using the formula $\Delta R_2(\theta) = R_{iso} + R_{ani}[Y_2^0(\theta,\varphi)]^2$, where R_{iso} is a scaling factor that depends on the amount of PhOH in binding modes (i) and (ii), R_{ani} is a scaling factor that depends on the amount of PhOH in binding mode (iii), and $Y_2^0(\theta,\varphi) = (1/4)\sqrt{(5/\pi)}(3cos^2\theta - 1)$ (Figure 2). θ is the angle formed by the C-H bond vector and the axis of rotation in binding mode (iii) (Figure 2d), which is responsible for the observed anisotropy in ΔR_2.[7] Note that, while the experimental ΔR_2 values depend on the angle θ, the modelled R_{iso} and R_{ani} values are global parameters characteristic of each phenolic compound. Errors on the modelled R_{iso} and R_{ani} values were computed by Monte Carlo simulation of synthetic datasets from the estimated experimental error on ΔR_2. Additional information on the modelling of the experimental ^{13}C ΔR_2 data is provided in the section "*Guide to interpretation of ^{13}C ΔR_2 data*".

Hydrogenation of Phenol. 10 mM PhOH solutions were prepared in deionized water, and the pH was adjusted to 7.0 ± 0.1 using dilute HCl or NaOH. In a typical reaction, the catalyst (10 mg, Pd:Substrate = 2.5 mol %) and PhOH solution (4 mL, 0.010 M) were added to a 10 mL glass tube. The tube was sealed with a septum and purged with H_2 for 5 min at a rate of 20 cm^3/min. After 5 min, the pressure relief needle was removed and the H_2 supply was stopped. The reaction tube was then placed in an oil bath preset at 35°C. The reaction tube was maintained at 35 °C under constant stirring (800 rpm) for 7 h. Then, the septum was removed, and the solution was extracted using ethyl acetate (1.0 mL 4 times). A 50 μL aliquot of the extracted solution was taken and added to 1.00 mL of ethanol along with a 4-methylbenzylalcohol internal standard (50 μL, 25 mM) and analyzed in an Agilent GC-MS instrument (7890A, 5975C) with a HP-5MS column. The run started at 60°C, held for 2 min, and the temperature was ramped to 150°C at 15°C/min. Then the temperature was ramped to 300°C at 20°C/min and finally it was held constant at 300°C for 3 min. % conversions were calculated based on the decrease in concentration of the starting

materials. The products formed by the hydrogenation reactions are shown in Supporting Figure S5.

Conflicts of interest

There are no conflicts to declare.

Acknowledgements

This work was supported by startup funds from Iowa State University to V.V., and funds from the U.S. Department of Energy, Office of Basic Energy Sciences, Division of Chemical Sciences, Geosciences, and Biosciences, through the Ames Laboratory Catalysis Science program to I.I.S. The Ames Laboratory is operated for the U.S. Department of Energy by Iowa State University under Contract No. DE-AC02-07CH11358.

References

1. Gharibi, M.; Zangeneh, F. T.; Yaripour, F.; Sahebdelfar, S., Nanocatalysts for conversion of natural gas to liquid fuels and petrochemical feedstocks. *Applied Catalysis A: General* **2012,** *443-444*, 8-26.

2. Moshfegh, A. Z., Nanoparticle catalysts. *Journal of Physics D: Applied Physics* **2009,** *42* (23), 233001.

3. Fawzi, N. L.; Ying, J.; Ghirlando, R.; Torchia, D. A.; Clore, G. M., Atomic-resolution dynamics on the surface of amyloid-beta protofibrils probed by solution NMR. *Nature* **2011,** *480* (7376), 268-72.

4. Fawzi, N. L.; Ying, J.; Torchia, D. A.; Clore, G. M., Kinetics of Amyloid β Monomer-to-Oligomer Exchange by NMR Relaxation. *J Am Chem Soc* **2010,** *132* (29), 9948-9951.

5. Mittermaier, A.; Kay, L. E., New tools provide new insights in NMR studies of protein dynamics. *Science* **2006,** *312* (5771), 224-8.

6. Palmer, A. G., 3rd; Kroenke, C. D.; Loria, J. P., Nuclear magnetic resonance methods for quantifying microsecond-to-millisecond motions in biological macromolecules. *Methods Enzymol* **2001,** *339*, 204-38.

7. Egner, T. K.; Naik, P.; An, Y.; Venkatesh, A.; Rossini, A. J.; Slowing, I. I.; Venditti, V., 'Surface Contrast' NMR Reveals Non-innocent Role of Support in Pd/CeO2 Catalyzed Phenol Hydrogenation. *ChemCatChem* **2020,** *12*, 4160–4166.

8. Egner, T. K.; Naik, P.; Nelson, N. C.; Slowing, II; Venditti, V., Mechanistic Insight into Nanoparticle Surface Adsorption by Solution NMR Spectroscopy in an Aqueous Gel. *Angew Chem Int Ed Engl* **2017,** *56* (33), 9802-9806.
9. Zhang, Y.; Xu, H.; Parsons, A. M.; Casabianca, L. B., Examining Binding to Nanoparticle Surfaces Using Saturation Transfer Difference (STD)-NMR Spectroscopy. *J. Phys. Chem. C* **2017,** *121*, 24678-24686.
10. Nelson, N. C.; Manzano, J. S.; Sadow, A. D.; Overbury, S. H.; Slowing, I. I., Selective Hydrogenation of Phenol Catalyzed by Palladium on High-Surface-Area Ceria at Room Temperature and Ambient Pressure. *ACS Catal* **2015,** *5*, 2051-2061.
11. Dotas, R. R.; Nguyen, T. T.; Stewart Jr., C. E.; Ghirlando, R.; Potoyan, D. A.; Venditti, V., Hybrid thermophilic/mesophilic enzymes reveal a role for conformational disorder in regulation of bacterial Enzyme I. *J Mol Biol* **2020,** *432*, 4481-4498.
12. Mai, H. X.; Sun, L. D.; Zhang, Y. W.; Si, R.; Feng, W.; Zhang, H. P.; Liu, H. C.; Yan, C. H., Shape-selective synthesis and oxygen storage behavior of ceria nanopolyhedra, nanorods, and nanocubes. *J Phys Chem B* **2005,** *109* (51), 24380-5.
13. de Oliveira, R. C.; Amoresi, R. A. C.; Marana, N. L.; Zaghete, M. A.; Ponce, M.; Chiquito, A. J.; Sambrano, J. R.; Longo, E.; Simões, A. Z., Influence of Synthesis Time on the Morphology and Properties of CeO_2 Nanoparticles: An Experimental–Theoretical Study. *Cryst. Growth Des.* **2020,** *20*, 5031–5042.
14. Amoresi, R. A. C.; Oliveira, R. C.; Marana, N. L.; de Almeida, P. B.; Prata, P. S.; Zaghete, M. A.; Longo, E.; Sambrano, J. R.; Simões, A. Z., CeO_2 Nanoparticle Morphologies and Their Corresponding Crystalline Planes for the Photocatalytic Degradation of Organic Pollutants. *ACS Appl. Nano Mater.* **2019,** *2*, 6513–6526.
15. Zhou, K.; Wang, X.; Sun, X.; Peng, Q.; Li, Y., Enhanced catalytic activity of ceria nanorods from well-defined reactive crystal planes. *J. Catal.* **2005,** *229*, 206-212.
16. Hu, Z.; Liu, X.; Meng, D.; Guo, Y.; Guo, Y.; Lu, G., Effect of Ceria Crystal Plane on the Physicochemical and Catalytic Properties of Pd/Ceria for CO and Propane Oxidation. *ACS Catal* **2016,** *6*, 2265-2279.
17. Lei, Y.; Li, W.; Liu, Q.; Lin, Q.; Zheng, X.; Huang, Q.; Guan, S.; Wang, X.; Wang, C.; Li, F., Typical crystal face effects of different morphology ceria on the activity of Pd/CeO2 catalysts for lean methane combustion. *Fuel* **2018,** *233*, 10-20.
18. Anthis, N. J.; Clore, G. M., Visualizing transient dark states by NMR spectroscopy. *Q Rev Biophys* **2015,** *48* (1), 35-116.

19. Li, G.; Han, J.; Wang, H.; Zhu, X. F.; Ge, Q., Role of Dissociation of Phenol in Its Selective Hydrogenation on Pt(111) and Pd(111). *ACS Catal* **2015,** *5*, 2009−2016.
20. Ceccon, A.; Tugarinov, V.; Bax, A.; Clore, G. M., Global Dynamics and Exchange Kinetics of a Protein on the Surface of Nanoparticles Revealed by Relaxation-Based Solution NMR Spectroscopy. *J Am Chem Soc* **2016,** *138* (18), 5789-92.
21. Sachleben, J. R.; Colvin, V.; Emsley, L.; Wooten, E. W.; Alivisatos, A. P., Solution-State NMR Studies of the Surface Structure and Dynamics of Semiconductor Nanocrystals. *J Phys Chem B* **1998,** *102*, 10117-10128.
22. Agarwal, S.; Mojet, B. L.; Lefferts, L.; Datye, A. K., Chapter 2 - Ceria Nanoshapes—Structural and Catalytic Properties. In *Catalysis by Materials with Well-Defined Structures*, Wu, Z.; Overbury, S. H., Eds. Elsevier: Amsterdam, 2015; pp 31-70.
23. Mann, A. K. P.; Wu, Z.; Overbury, S. H., Chapter 3 - The Characterization and Structure-Dependent Catalysis of Ceria with Well-Defined Facets. In *Catalysis by Materials with Well-Defined Structures*, Wu, Z.; Overbury, S. H., Eds. Elsevier: Amsterdam, 2015; pp 71-97.
24. Hao, X.; Yoko, A.; Chen, C.; Inoue, K.; Saito, M.; Seong, G.; Takami, S.; Adschiri, T.; Ikuhara, Y., Atomic-Scale Valence State Distribution inside Ultrafine CeO2 Nanocubes and Its Size Dependence. *Small* **2018,** *14* (42), e1802915.
25. Tan, Z.; Li, G.; Chou, H. L.; Li, Y.; Yi, X.; Mahadi, A. H.; Zheng, A.; Tsang, S. C. E.; Peng, Y. K., Differentiating Surface Ce Species among CeO_2 Facets by Solid-State NMR for Catalytic Correlation. *ACS Catal* **2020,** *10*, 4003-4011.
26. Zhou, H.; Wang, H.; Sadow, A. D.; Slowing, I. I., Toward hydrogen economy: Selective guaiacol hydrogenolysis under ambient hydrogen pressure. *Appl Catal B* **2020,** *270*, 118890.

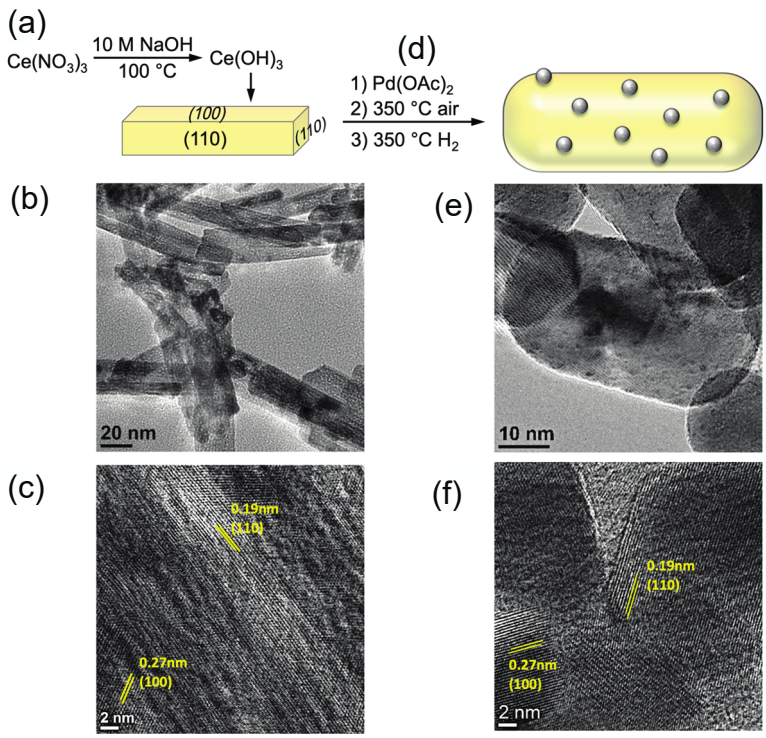

Fig. 1. CeO_2 and Pd/CeO_2 nanorods. (**A**) Scheme representing the synthesis of CeO_2 nanorods, and their corresponding (**B**) TEM and (**C**) HR TEM images. (**D**) Production of Pd/CeO_2 nanorods and their corresponding (**E**) TEM and (**F**) HR TEM images. Both materials expose predominantly (110) and (100) planes.

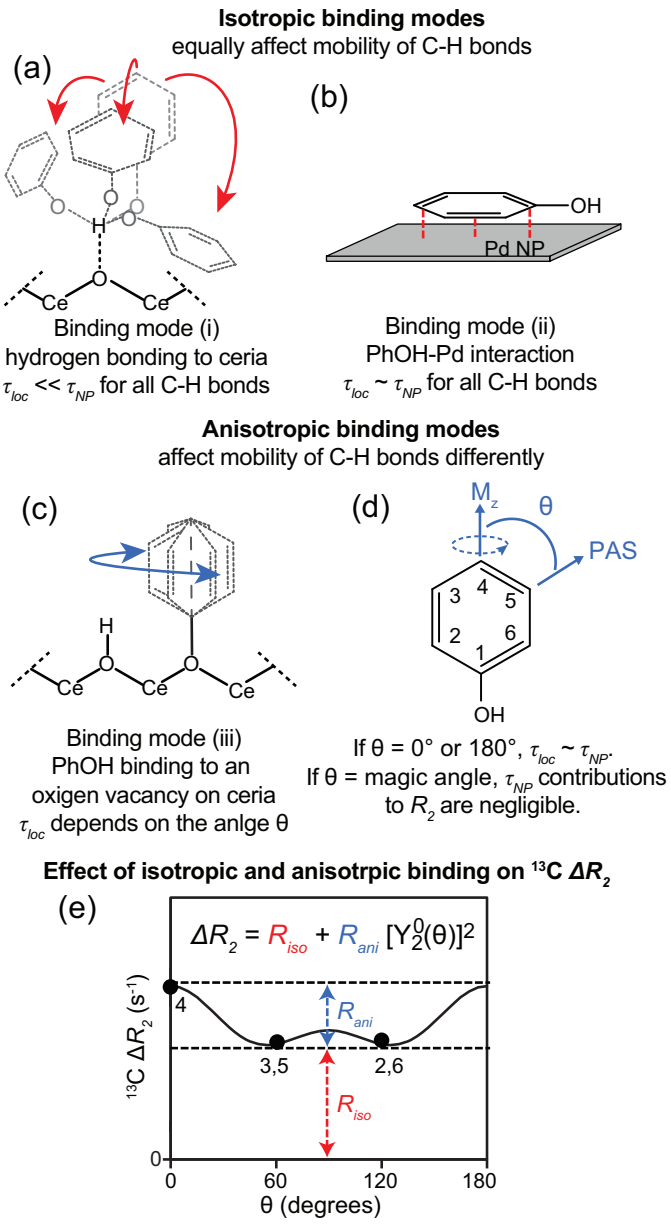

Fig. 2. Interpretation of ^{13}C ΔR_2. Structural models for (**A**) PhOH hydrogen-bonded to ceria, (**B**) PhOH adsorbed on a Pd NP site, and (**C**) PhOH bound to an oxygen vacancy on ceria. Binding modes in (A) and (B) (referred to as binding modes (i) and (ii) in the text) induce homogeneous ^{13}C ΔR_2 across the molecule (isotropic binding modes). (**D**) The binding mode in (C) (referred to as binding mode (iii) in the text) results in a dependency of the ^{13}C ΔR_2 from the angle θ formed by the principle axis system of the relaxation vector (i.e. the C-H bond vector, PAS) and the axis of the restricted rotation (i.e. the axis of the C-O bond, M_z) (anisotropic binding mode). (**E**) In the presence of binding modes (i)-(iii),

the dependency of ^{13}C ΔR_2 on θ can be modelled by optimizing the values of the parameters R_{iso} and R_{ani} that are proportional to the population of PhOH in the isotropic or anisotropic binding modes, respectively.

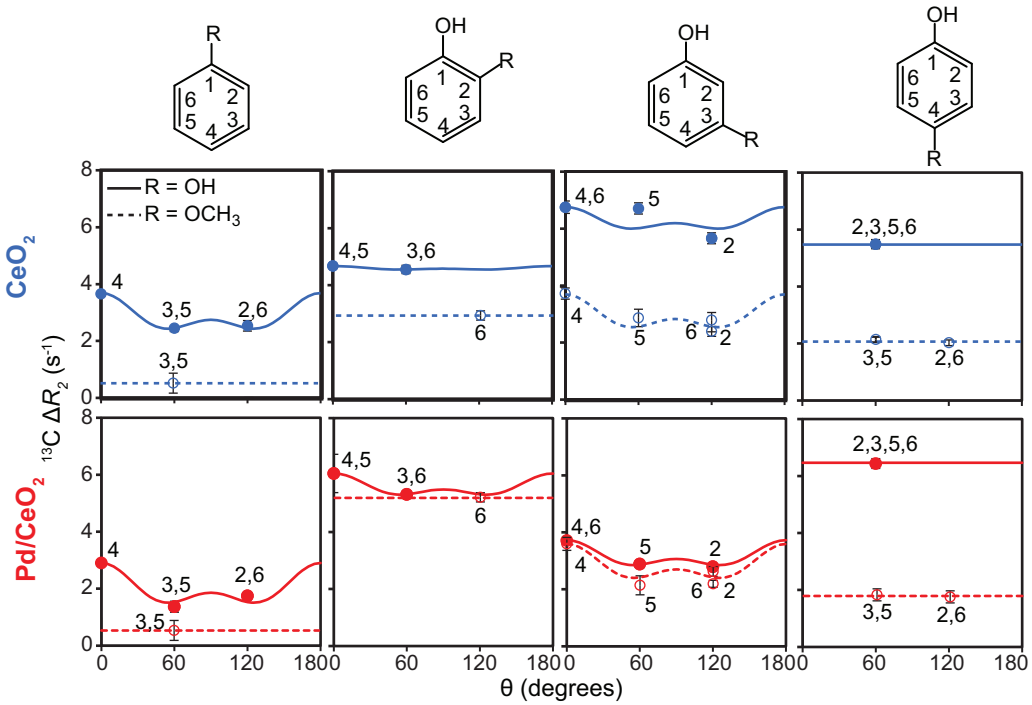

Fig. 3. Experimental ^{13}C ΔR_2 versus θ. ^{13}C ΔR_2 measured for PhOH, anisole, and the hydroxy and methoxy derivatives of PhOH upon addition of CeO_2 (top, blue) and Pd/CeO_2 (bottom, red) are plotted versus the angle θ. Experimental data are shown as filled and open circles for R = OH and R = OCH_3, respectively. Modelled data are shown as solid and dashed lines for R = OH and R = OCH_3, respectively. ^{13}C ΔR_2 for the 2, 4, and 6 positions of anisole and for the 3, 4, and 5 positions of 2-methoxyphenol were not measured due to NMR signal overlap (Supporting Figure S4).

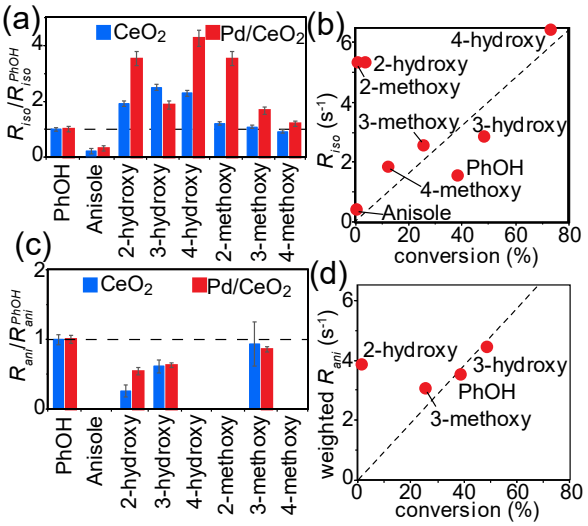

Fig. 4 Correlation between NMR data and catalytic conversion. (**A**) Bar graph showing the R_{iso} parameters optimized from the ^{13}C ΔR_2 data measured for PhOH, anisole, and the hydroxy and methoxy derivatives of PhOH upon addition of CeO_2 (blue bars) and Pd/CeO_2 (red bars). Data are normalized respect to the R_{iso} parameter measured for PhOH (R_{iso}^{PhOH}). Numerical values of R_{iso} are listed in Table 1. (**B**) R_{iso} parameters obtained upon the addition of Pd/CeO_2 are plotted versus the % conversions measured by incubating the small molecule substrates with 1 wt% Pd/CeO_2 at 35 °C and 1 bar H_2 for 7 h. (**C**) Bar graph showing the R_{ani} parameters optimized from the ^{13}C ΔR_2 data measured for PhOH and its hydroxy and methoxy derivatives upon addition of CeO_2 (blue bars) and Pd/CeO_2 (red bars). Data are normalized respect to the R_{ani} parameter measured for PhOH (R_{ani}^{PhOH}). Numerical values of R_{ani} are listed in Table 1. R_{ani} for anisole, 4-hydroxyphenol, 2-methoxyphenol, and 4-methoxyphenol were not optimized do the impossibility of measuring ΔR_2 for θ = 0° (see main text). (**D**) R_{ani} parameters obtained upon the addition of Pd/CeO_2 are plotted versus the % conversions measured by incubating the small molecule substrates with 1 wt% Pd/CeO_2 at 35 °C and 1 bar H_2 for 3 h. R_{ani} for the hydroxyphenols were multiplied by 2 in order to compensate for the ambiguity in the definition of the position with θ = 0° (see main text).

Table 1. Optimized R_{iso} (s^{-1})[a] and R_{ani} (s^{-1})[a] parameters.

	phenol		**anisole**		**2-hydroxy phenol**		**2-methoxy phenol**		**3-hydroxy phenol**		**3-methoxy phenol**		**4-hydroxy phenol**		**4-methoxy phenol**	
	R_{iso}	R_{ani}	R_{iso}	R_{ani}	R_{iso}	R_{ani}	R_{iso}	R_{ani}	R_{iso}	R_{ani}	R_{iso}	R_{ani}	R_{iso}	R_{ani}	R_{iso}	R_{ani}
CeO_2	2.6	3.1	0.5	-	4.6	0.6	2.9	-	6.0	1.9	2.6	2.9	5.5	-	2.2	-
Pd/CeO_2	1.5	3.5	0.6	-	5.3	1.9	5.3	-	2.8	2.2	2.5	3.0	6.4	-	1.8	-

[a]Errors are ≤ 0.1 s^{-1} in all cases.

Table of content

Selective Phenol hydrogenation by Pd/CeO_2